

Transformation of molecular oxygen on a platinum surface: A theoretical calculation of STM images

M.-L. Bocquet

*Laboratoire de Chimie Théorique, Ecole Normale Supérieure, 46 Allée d'Italie, 69364 Lyon Cedex 07, France
and Institut de Recherches sur la Catalyse, CNRS, 2 Avenue Albert Einstein, 69626 Villeurbanne Cedex, France*

J. Cerdà

Instituto de Ciencia de Materiales de Madrid, CSIC, Cantoblanco, 28049 Madrid, Spain

P. Sautet*

*Laboratoire de Chimie Théorique, Ecole Normale Supérieure, 46 Allée d'Italie, 69364 Lyon Cedex 07, France
and Institut de Recherches sur la Catalyse, CNRS, 2 Avenue Albert Einstein, 69626 Villeurbanne Cedex, France*

(Received 29 October 1998)

Using the recently modified electron scattering quantum chemical approach, we have performed simulations of the scanning tunneling microscope (STM) image contrast associated with elementary steps of O₂ dissociation on platinum(111). Two metastable molecular precursors, binding to different adsorption sites, and the stable atomic species have been studied. The two molecular chemisorbed structures have been identified very recently with a low-temperature STM. From density-functional-theory calculations, which allow a full geometry optimization of the adsorbate and the surface, two molecular precursors adsorbed at the fcc hollow and bridge sites have very similar chemisorption energy. In the calculated STM image, with a tip ending with a Pt atom, the O₂ molecule and the O atom appear as a depression, which only agrees with the experiment in the case of the O atom. However, the image is found to be strongly dependent on the value of the gap resistance and on the termination of the tip. A tip ending with a CO molecule, which models a tip contaminated with an adsorbate, gives images in good agreement with the experimental results. [S0163-1829(99)02823-4]

I. INTRODUCTION

The scanning tunneling microscope (STM) has proven to be an exceptional tool for the study of adsorbates at metallic or semiconducting surfaces. Images of individual molecules or dense layers can be obtained with molecular resolution. It has been shown that the internal structure of the molecule STM pattern is not directly related to the atomic structure but depends on the bonding site at the surface.¹ It is therefore clear that the shape of the molecular feature on the image cannot be directly related to the molecular geometry and nature. A theoretical calculation is then needed in order to understand the relation between image and structure.

Molecules do not only chemisorb at surfaces, they also transform and react. The fundamental knowledge of these elementary reactions at surfaces is of large interest to the applied fields of catalysis, corrosion, etc. It is clear that the time scale for the chemical transformation itself is much shorter than the STM acquisition time. However, metastable intermediates of the transformation can be frozen and imaged with a variable low-temperature STM. The transformation of molecular oxygen on a Pt(111) surface is a case of special interest because it presents a variety of adsorbate structures with different strengths in the adsorbate-substrate interaction. The key point is whether the STM is able to follow the chemical transformation of this molecule in contact with a platinum surface, and to recognize the different metastable intermediates by assigning each to a particular image pattern. It is also important to understand under which condition recognition with the STM of these intermediates is possible, and to address the influence of the general experi-

mental parameters such as the gap resistance and the tip termination.

In Sec. II, previous experimental and theoretical studies are summarized, with a special emphasis on the recent STM experiment. In Sec. III, the results of our density-functional-theory (DFT) calculations on the structure and energy of the precursor and dissociated states are described. Maps of the local density of states at the Fermi level are shown, and they can be seen as a first approximation to the STM images in the framework of the perturbative Tersoff-Hamman approach. In Sec. IV, our scattering theory approach to STM image calculations is briefly summarized, and the simulated images for the oxygen species on Pt(111) are presented. Finally, in Sec. V, the influence of the gap resistance and of the tip apex structure on the calculated images is addressed.

II. OVERVIEW OF THE EXPERIMENTAL AND THEORETICAL STUDIES ABOUT O₂ ON Pt(111)

At very low temperature ($T < 40$ K), O₂ physisorbs on the surface with a structure unchanged compared with the gas-phase structure. At higher temperature, first one² and later two³ distinct chemisorbed structures have been found experimentally, with different bonding sites at the surface and activation of the O-O bond. The first chemisorption is described as a π interaction with an O-O elongation of 0.16 Å, while the second situation yields more charge transfer toward the antibonding molecular orbitals and corresponds to a σ interaction, with a 0.23-Å bond-length increase. At a temperature above 150 K the molecule is dissociated, and atomic

oxygen is found on the surface with a threefold adsorption site.

A low-temperature STM study recently appeared.⁴ Two types of chemisorbed O_2 species on a flat (111) terrace on platinum were resolved. One molecular feature resembles a “four-leaf clover” shape centered on bridge sites, and was assigned to a superoxo O_2^- species. The other O_2 molecule is positioned at a hollow site, and the image has a “pear shape” with a bright lobe in the direction pointing to the top site. The authors conclude from comparison with previous spectroscopic studies⁵ that this structure has a weaker O-O bond. A third molecular feature has also been found at the terrace edges, and it appears as two lobes centered on the bridge site. These three positive molecular features are always surrounded by a lateral depression compared to the bare surface. With an increase of the bias voltage and tunnel current, dissociation of individual molecules on the surface was induced, leading to a strong change in the STM contrast of the adsorbates. Depending on the chosen image, atomic oxygen appears as a hole, in agreement with previous studies,⁶ or with a small bump in the middle of the hole. When the oxygen is seen as a simple hole, no atomic resolution is achieved on the bare surface, while in the images where oxygen presents a bump in the middle of the hole, individual Pt atoms are clearly seen on the substrate. This strongly suggests that this second type of image has been obtained with a contaminated tip apex. Important conclusions stem from this paper. Two molecular precursors coexist on the surface, assigned to bridge and fcc hollow adsorption. Three different image shapes have been shown that need to be precisely interpreted.

The chemisorption of O_2 on Pt(111) has been the subject of theoretical studies. In the earliest one, with a semiempirical approach,⁷ the most favorable molecular site was found to be the bridge site, with the O-O axis parallel to the surface, and to the Pt-Pt bond. More recent DFT studies⁸ showed that two molecular precursors exist: one on the bridge site and one on the hollow site, in very good agreement with the STM results. Very recently, results from a tight-binding molecular dynamics simulation were published.⁹ In contrast with previous studies, a low-symmetry site was proposed, while STM images are simulated with a Tersoff-Hamann approach.¹⁰

III. STRUCTURAL DETERMINATION OF THE MOLECULAR AND ATOMIC CHEMISORBED STATES

Our calculations are based on density-functional theory and the use of a spin-polarized version of the Vienna *ab initio* simulation program (VASP).^{11,12} The code gives an iterative solution of Kohn-Sham equations of local-spin density, in a plane-wave basis set and using fully nonlocal Vanderbilt-type ultrasoft pseudopotentials to describe the electron-ion interaction.¹³ Nonlocal corrections are added in the form of the generalized gradient approximation (GGA) of Perdew *et al.*¹⁴

In relation to the ultrasoft pseudopotentials, a cutoff for the plane-wave expansion of 400 eV was selected, assuring a very good convergence of the energy. The Pt(111) surface is modeled by a four-layer slab, with a 2×2 surface cell. A supercell geometry is used, and slabs are separated by a

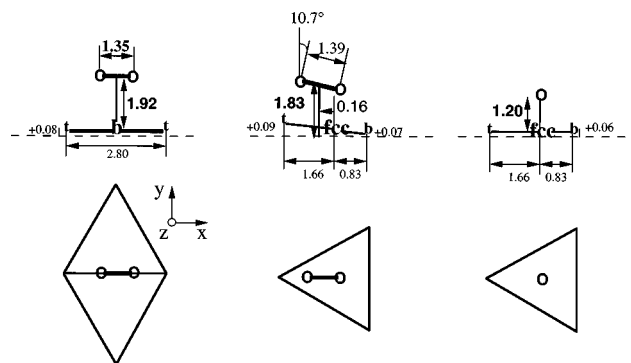


FIG. 1. Optimized structures of the two chemisorbed molecular precursors and of the atomic dissociation state for oxygen on Pt(111). These geometries result from GGA local-spin-density calculations including a relaxation of the adsorbate and the substrate (two outer layers).

vacuum gap equivalent to four Pt layers. A single oxygen molecule is introduced on one side of the slab, and thus represents a 0.5-ML coverage as in the experimental studies. Brillouin-zone integrations have been performed on a grid of $5 \times 5 \times 1$ k points, using a Methfessel-Paxton smearing of $\sigma = 0.25$ eV. The adsorbate and two outer Pt layers are allowed to relax until the largest residual force is less than $0.1 \text{ eV } \text{Å}^{-1}$, as usual for similar calculations. The other two Pt layers adopt a fixed geometry with the equilibrium lattice constant $a = 4 \text{ Å}$, which corresponds to a Pt-Pt bond length of 2.82 Å .

The O_2 molecule is chemisorbed with the O-O axis more or less parallel with respect to the surface. We have calculated the molecular adsorption on four classical symmetry sites (hcp hollow, fcc hollow, bridge, and top) together with two possible azimuthal orientations of the molecular axis (parallel and perpendicular to the Pt atomic rows), and we present only the most stable situations, i.e., the fcc and hcp perpendicular hollow structure and the parallel bridge one. We have also optimized the geometry for an atomic oxygen, which prefers to be on a fcc hollow site.

In Fig. 1, the geometrical results of the calculations are schematically drawn. Only one hollow site is depicted, since they yield a similar chemisorption structure. The bridge O_2 species lies flat on the surface, with a moderate elongation of the O-O bond length compared to the gas-phase molecule ($+0.11 \text{ Å}$). For the hollow sites, the O_2 molecule is perpendicular to Pt rows, its center is shifted 0.16 Å toward the top site, and the oxygen atom near the top is 0.26 Å higher than the atom near the bridge. The O-O bond is elongated by 0.15 Å . For all sites, we observe a small but significant geometric relaxation of the surface atom neighbors of the adsorbate (in-plane and out-of-plane displacements are smaller than 0.1 Å). Let us now discuss the energy results. The adsorption energies are compiled in Table I. The adsorption energy is defined as the difference between the energy of the chemisorbed system (final state) and the energy of the initial state. For molecular (respectively atomic) oxygen, this initial state energy is the sum of the energy of the clean Pt system and of the energy (half the energy) of the “isolated” oxygen molecule in the same box. We distinguish the results with and without taking substrate relaxation into account. This relaxation does not change the molecular geometry but stabilizes

TABLE I. Calculated chemisorption energy (in eV) for the molecular precursors and the atomic adsorption for oxygen on Pt(111). The influence of surface relaxation is underlined>.

Adsorption energy (eV)	Without/ <u>with</u> surface relaxation
O ₂ bridge	-0.53/-0.64
O ₂ hcp hollow	-0.40/-0.46
O ₂ fcc hollow	-0.47/-0.65
O fcc hollow	-0.86/-1.08

the adsorbed structures in a nonequivalent way.

For the molecular chemisorption, the fcc hollow site and the bridge site are found to be the most stable ones. If surface relaxation is not taken into account, the bridge site is favored by 60 meV. The situation is reversed when surface relaxation is allowed, and the fcc hollow site becomes 10 meV more stable. Those differences are small but, to our knowledge, this is one of the first times that substrate relaxation is shown to yield a change in the most stable chemisorption site. The two sites therefore have a very similar chemisorption energy which is consistent with their coexistence on the surface.

In agreement with experiment, we find the hcp hollow site to be less stable (about 200 meV less). Among all the considered structures only the bridge site chemisorption shows a residual spin polarization on the O₂ molecule (0.89 μ b). These results show small differences compared to a previous study by Eichler and Hafner⁶ with the same code. Those differences arise from non equivalent calculation conditions. For example a $c(4 \times 2)$ unit cell [instead of (2×2)] and a smaller K mesh was used in this previous study.

Two-dimensional maps of charge density in a plane parallel to the surface over the chemisorbed system have been calculated, and are represented in Fig. 2. States within an energy interval of 0.1 eV centered at the Fermi level were considered, and the plane was positioned at a 4-Å distance from the Pt surface. If the perturbative approach of Tersoff and Hamman¹⁰ is considered, these plots are models of the STM images. All adsorbates appear as a clear protrusion with no depression around them. The structures are associated with enhanced charge density on the adsorbates compared to the naked metallic surface. The two molecular precursors give images that compare reasonably well with experiment for the fcc hollow site with a pear shape feature, but less for the bridge site, where a double bump is seen in the calculations. The agreement is however not satisfactory for the oxygen atom, where a marked bump appears in the charge density image: oxygen has been repeatedly imaged as a hole (eventually with a bump in the middle of the hole) on several metals.^{15,16} The reason for this discrepancy could be the absence of a precise description of the tip apex electronic structure in this model and/or the distance (4 Å) between a hypothetical tip and the surface which is far too close compared to common experimental conditions (7–8 Å). Larger distances cannot be reached with VASP due to accuracy problems in the small charge density far from the surface.

IV. STM IMAGES OF THE SEQUENCE OF INTERMEDIATES

In order to simulate STM images, calculations of the tunnel current have been performed with a scattering matrix

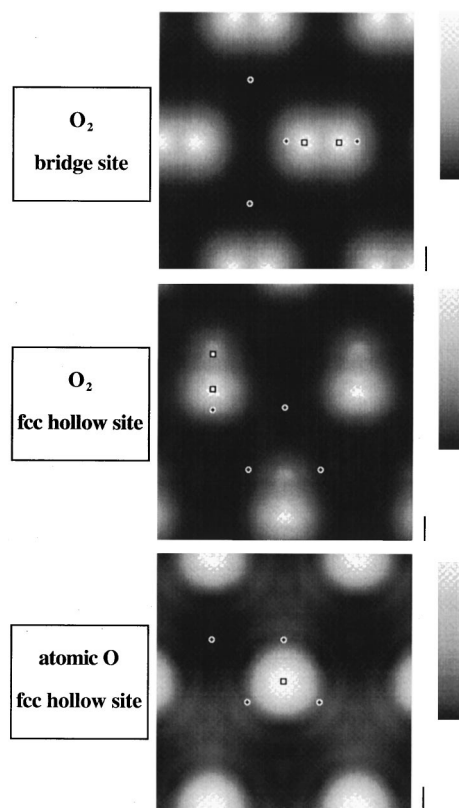


FIG. 2. Fermi-level charge density, obtained from the DFT calculations, in a plane parallel to the surface at a 4-Å distance from the Pt surface layer. The three structures of Fig. 1 are considered: O₂ in a bridge site (top), O₂ in a fcc hollow site (middle), and atomic O in a fcc hollow site (bottom). The black-to-white scale is associated with the minimum-to-maximum amplitude values. The positions of oxygen atoms (and some Pt atoms) are labeled with square (cross) markers.

approach already detailed in previous papers.¹⁷ The system is described by two semi-infinite Pt solids ending with two (111) surfaces separated by a gap. On one side (the surface) a periodic chemisorption of an O₂ molecule (or O atom) in a 5×5 cell is considered, in order to model an ‘‘isolated’’ adsorbate. On the other side of the gap, a tetrahedral cluster of Pt atoms pointing toward the surface is positioned in order to model the metallic tip.

A set of atomic orbitals is associated to each atom and the effective semi-empirical extended Hückel technique¹⁸ is used in order to calculate the Hamiltonian matrix elements. The tunnel current is calculated from the electronic scattering matrix and the Landauer¹⁹ approach. Compared to previous studies, the procedure for the calculation of the scattering matrix has been modified from a propagative to a generalized Green-function formalism.²⁰ This algorithm presents, as main advantages, the possibility to treat a bias voltage beyond linear response in the current, accurate integrations over the two-dimensional Brillouin zones both at the substrate and the tip, and an improved computational efficiency and stability. Here a small 10-mV bias voltage has been considered, and no effect on the STM contrast was noted compared to the zero-bias limit, as could be expected. For the surface and tip, a set of 100 K points was selected, corresponding to 400 K points for the Pt bulk two-dimensional

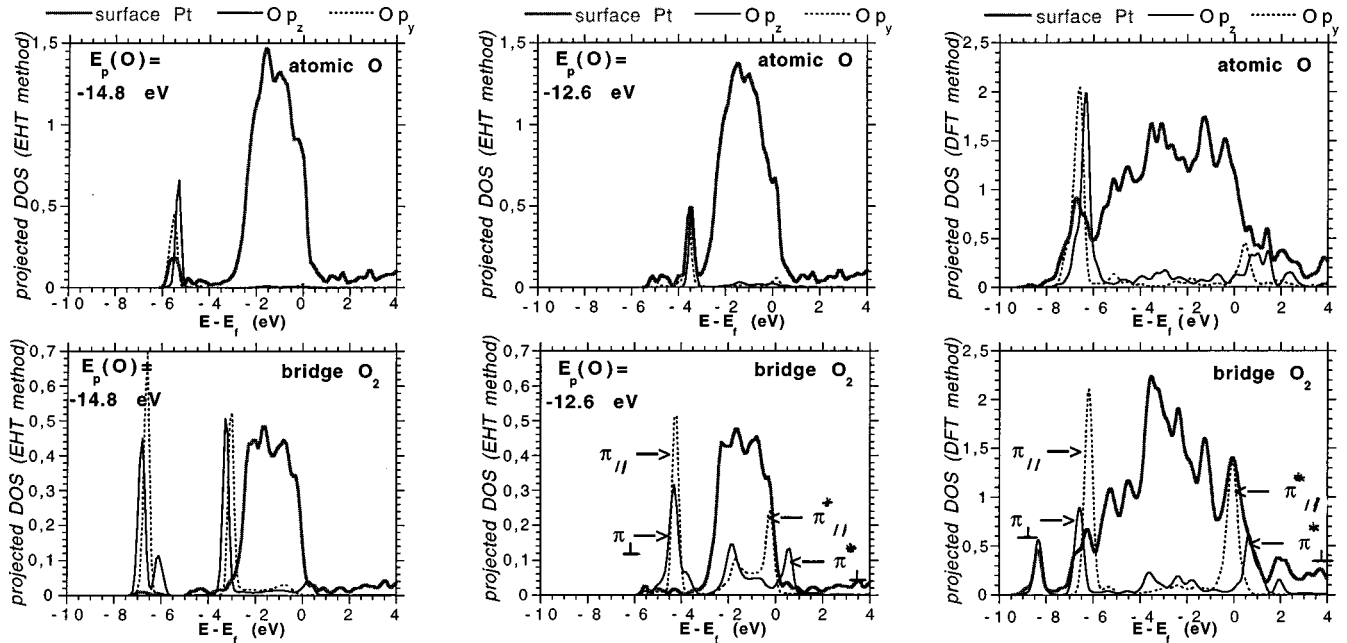


FIG. 3. Atom-projected densities of states for atomic oxygen (top) and the bridge site O_2 molecule on Pt(111). The DFT result (right) is compared to the extended Hückel calculations with a standard $O 2p$ orbital energy (-14.8 eV, left) or a less negative shifted value (-12.6 eV, middle). Energies are relative to the Fermi level. The following projections are given: Pt atom (bold gray), $O 2p_y$ orbital (full line), and $O 2p_z$ orbital (dashed line).

Brillouin zone, and assuring a good convergence. A Slater-type basis set of atomic orbitals was considered: Pt atoms in the substrate and tip bulks are only represented by a $6s$ basis, while in the gap region (one surface layer, adsorbates, and a tip cluster) full valence $5d$, $6s$, and $6p$ bases are used for Pt and $2s$ and $2p$ bases for O. The atoms in the gap region are described by a double ζ Slater basis set in order to better describe the long-range interaction in the tunnel junction. The orbital exponents are obtained from atomic calculations²¹ and the orbital energies are taken from the literature.²² The only parameter that we have adjusted is the orbital energy of the oxygen $2p$ level, that was moved from -14.7 to -12.6 eV. This allows us to raise the energy of the O_2 and O levels, decrease the charge transfer toward the adsorbate, and significantly improve the comparison between the DFT and semiempirical one-electron structures. This is illustrated in Fig. 3, where partial densities of states (DOS's) are compared. A projection is given on the Pt atom interacting with the adsorbate, and on the p_y and p_z orbitals of the O atoms which describe the O-O π system (for axis labels, see Fig. 1). The two first columns correspond to the extended Hückel approach (with -14.8 or -12.6 eV for the $O 2p$ orbital energy), while the third one corresponds to the DFT calculations. The Pt d -band-width is narrower in the extended Hückel calculation, which can be associated to a scale factor in the energy axis. However, the relative positions of the oxygen-induced features are well reproduced with respect to the Pt d band and the Fermi level, if the modified -12.6 -eV $O 2p$ energy is selected, and the semiempirical partial DOSs are in qualitative agreement with the DFT ones. In the case of atomic oxygen, the $O 2p$ peaks are located at the lower Pt d -band edge. In the case of O_2 , the π levels are right below the Pt d band while the antibonding π^* peaks are in the vicinity of the Fermi level. The good agreement between DFT and semiempirical results for the electronic

structure close to the Fermi level is especially relevant here, since the scattering channels for the STM simulation are taken at the Fermi level. This shows that, despite its simplicity, this approach grasps the main qualitative features of the electronic structure for oxygen on Pt(111).

Calculated images for the bridge and fcc hollow molecular O_2 precursors and for the final dissociated state are reproduced in Fig. 4. The molecular species appear as a clear depression elongated along the O-O bond, in contrast with the bump shape from the data of Stipe *et al.*⁴ The fcc hollow site only shows a weak feature in the middle of the hole. The asymmetry between the two O atoms is mainly a geometrical effect due to the different adsorption heights of the two atoms, since, if we suppress the tilt of the molecular axis, this internal feature disappears leading to a simple elliptic depression along the O-O axis. The oxygen atom also appears as a spherical hole, this time in agreement with several experimental observations.

Let us explain the origin of the depressions for these calculated images of precursors. In fact, our approach provides an interpretation of the current based on the decomposition of the interactions within the tunnel gap. As in previous studies,²³ a clear and simple physical insight is obtained by decomposing the current into through-molecule and through-surface contributions, respectively, arising from the tip-molecule and tip-surface interactions. This contrast decomposition is performed on current cross sections, as shown in Fig. 5. The tip-surface separation is kept constant for the three chemisorption cases, at a value of 7.2 \AA giving a current of 1 nA for a bias of 10 mV for the bare surface.

The atomic contrast has already been detailed in a previous paper,¹⁶ and here we focus on the chemisorbed states. In Fig. 5 we show that the presence of the adsorbate induces a depression in the through-surface current, by perturbation of the surface atoms; this depression is important for the mo-

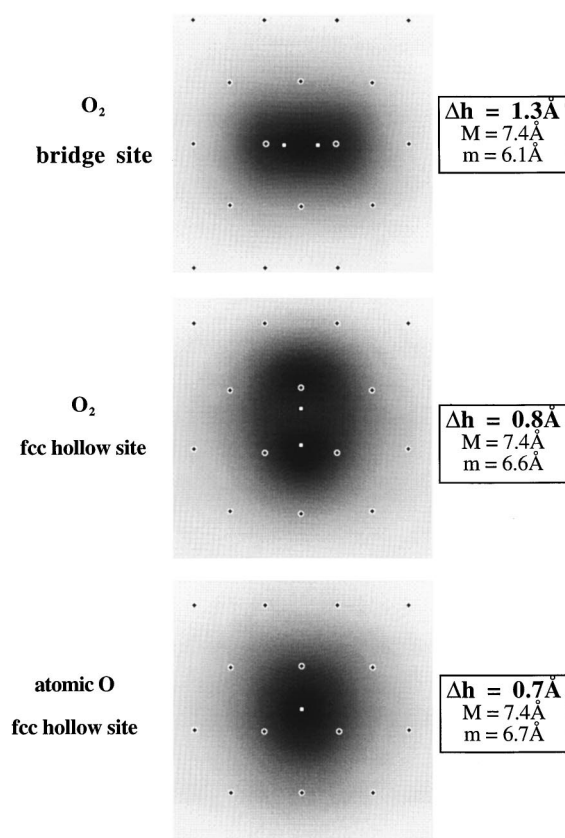


FIG. 4. $10 \times 10\text{-}\text{\AA}^2$ STM topographic computed images (bias 10 mV, current 1 nA, Pt tip) together with their minimum (m) and maximum (M) z values. The overall image corrugation Δh is also given. The geometries are the relaxed ones drawn in Fig. 1. Labels for the atom positions are the same as in Fig. 2. The black-to-white scale is associated with the minimum-to-maximum tip z values.

molecular and atomic chemisorption, but would be negligible for a weaker interaction such as a physisorbed state. In fact, as soon as the molecule draws close to the surface, allowing substantial orbital overlaps, the metallic states at the surface are consequently shifted away from the bulk levels. This energetic shift cancels the resonance with the bulk states, and the resulting current is thus decreased. Hence, as soon as this interaction is strong enough, the through-surface contribution creates a hole in the image. A through-molecule current is also induced. This through-molecule current is reduced when the molecule approaches the surface for a given tip height, and the nature of the molecular orbitals, important for tunneling, is changed from σ to π orbitals. Oxygen, which is an electronegative element, has contracted atomic orbitals. Therefore for the atomic and molecular chemisorption, the height difference between the oxygen and the surface is not able to counterbalance the important orbital expansion change between oxygen and platinum orbitals. The through-molecule current is hence not strong enough to compensate for the hole created in the through-surface current. This is why all adsorbate contrasts are negative, reflecting the perturbation of the surface metal atoms by the adsorbate.

Moreover, the shape and amplitude of the through-molecule current greatly depends on the adsorption site. In the chemisorbed bridge case, a double-lobe shape is found,

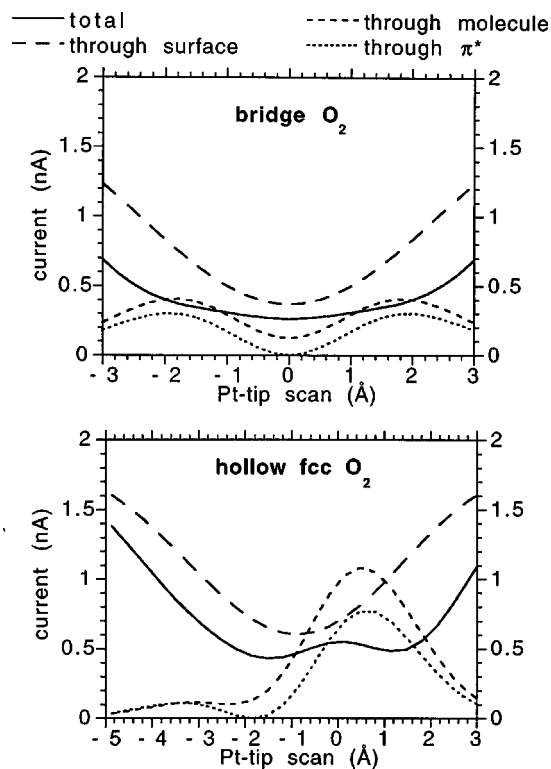


FIG. 5. Current (solid line) for a scan along the O-O direction centered on the molecule for a fixed tip height (7.2 \AA) relative to the surface, and for a bias voltage of 10 mV. The current is decomposed through surface (long dashed line), molecule (dashed line), and π^* molecular-orbital (dotted line) contributions.

the bumps being located 2 \AA away from the molecule center (it should be noted that the interlobe distance is much longer than the O-O bond length). The double-lobe pattern reflects the predominance of antibonding orbitals, that have a nodal plane bisecting the molecule and could correspond to the two positive experimental images (four-leaf clover and double bump) if their amplitudes were not masked by the through-surface contribution. The same conclusion stands for the hollow chemisorbed O_2 , with a pear shape through-molecule current, which is mostly masked by the large depression in the through-surface contribution. The final information provided by Fig. 5 is that the two current components, through-surface and through-molecule, are combined with a strong destructive interference effect. The main consequence of this destructive interference is to enlarge the hole associated with the chemisorbed states.

The key point for the resulting contrast of the molecule is therefore the balance between the through-surface and through-molecule currents. The simulation presented in Fig. 4 is dominated by the through-surface component, which imposes its depression in a way certainly exaggerated compared to the published images. It is therefore important to understand which parameter in the STM experiment and calculations can influence this balance.

Three effects have been tested: the substrate relaxation, the contamination of the tip apex, and the tunneling resistance. Images presented in Fig. 4 already include the relaxation of the substrate for the chemisorbed species determined by our *ab initio* calculations. This geometrical effect has a very minor influence on the contrast. For both sites, the re-

laxation slightly reduces the amplitude of the contrast. Conversely, the last two parameters which are related to experimental conditions have a great influence on the image.

V. INFLUENCE OF EXPERIMENTAL STM PARAMETERS ON THE CALCULATED IMAGES

When looking carefully at the published experimental images, we have already noted in Sec. II that the images of atomic oxygen and the resolution of the metal substrate atoms can vary in a significant way. A different atomic structure at the tip apex could explain these variations. Another way to modify the image contrast, and presumably to raise the through-molecule contribution, is to move the tip closer to the surface, which means tunneling at a lower gap resistance.

In Fig. 4, the resistance was fixed at a value of 10 M Ω . In Fig. 6, the influence of a decrease of the gap resistance in the calculated image topography is shown for the same Pt tip apex. The considered range of gap resistance 0.1–10 M Ω includes the domain of the experimental images (1–10 M Ω). Scans across the molecule, along the O-O direction and across the atoms, are given. All cases show an enhancement of the through-adsorbate contribution. For the molecule, shoulders appear within the depression already at a resistance of 1 M Ω and local maxima when the tip draws closer. Features from the molecule are then visible at low gap resistance, but the effect is not strong enough to yield a real contrast reversal, and the molecule area is still lower than the bare surface in the topographic image. Moreover the gap resistance value in order to observe the effect is smaller than the experimental ones. No contrast change is evidenced for the O atom in the range of tunnel resistance considered.

In order to model contamination, two different tip apex structures are considered in Fig. 7 for the same values of the gap resistance as in Fig. 6. The first tip is an oxygen-atom-terminated tip, where the Pt apex atom has been substituted by an O atom, therefore chemisorbed on the hollow site of the Pt₃ tip base unit. In the second tip, all four Pt atoms have been kept in the tip apex tetrahedron, but a CO molecule has been vertically chemisorbed by the C atom at the tip apex atom. Such a situation should be rather stable, since it was shown on stepped surfaces that CO binds more strongly at low coordination sites. Such tip apexes have been created by manipulation of CO molecules on a Cu(111) surface.²⁴ In all cases, the topographic *z* value is defined by the separation between the Pt surface layer and the lowest atom at the tip.

This change in the tip apex has a strong influence on the resulting STM image contrast. The contribution of the molecule is greatly enhanced compared to that of the bare surface, and the contrast reverses to positive for tunnel resistances that compare well with the experimental values. The effect is even more marked in the case of the CO tip, and the molecule is the brightest area of the image at a 1-M Ω resistance. A reduced gap resistance and a contaminated apex have therefore roughly the same effect of enhancing the molecular contribution, and these effects cumulate. For the case of the O atom on the surface, the effect is smaller, but a feature clearly appears at the bottom of the hole for the CO tip and for the O tip at very low resistances.

A set of images with a CO tip apex and a gap resistance

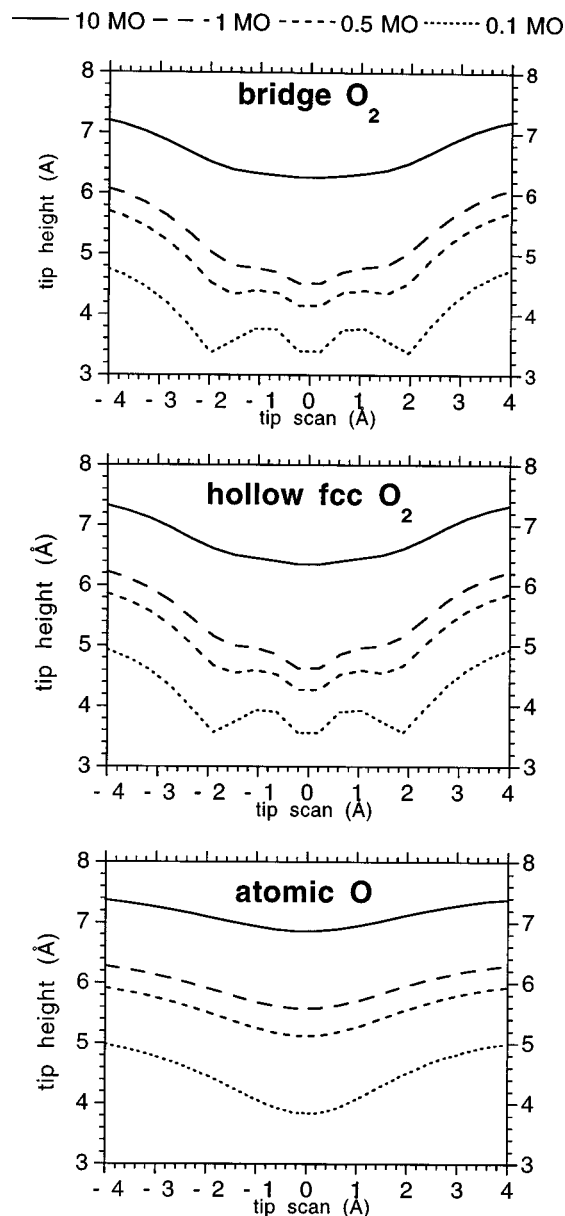


FIG. 6. Influence of the tunnel gap resistance. Topographic scans along the O-O bond for different values: 10 M Ω (solid line), 1 M Ω (long dashed line), 0.5 M Ω (dashed line), and 0.1 M Ω (dotted line). The tip ends with a Pt atom.

of 0.5 M Ω is shown in Fig. 8. The contrast is very different from that of Fig. 4, and clearly illustrates the enhancing of the molecular pattern. A good agreement is obtained here with the experimental images: The bridge site shows two lobes elongated in the direction perpendicular to the O-O bond which resembles a four-leaf clover. The fcc hollow site molecule appears asymmetric with a bright bump and a dimer area. All molecular features are surrounded by a depression. The image of the O atom is a hole with a bump in the middle of the hole, and corresponds well with the experimental images of Ref. 4.

Figure 9 shows the decomposition of the current for a fixed tip height into the through-surface and the through-molecule contributions to the current. The tip is the CO-terminated tip, and its *z* is selected to obtain a similar total

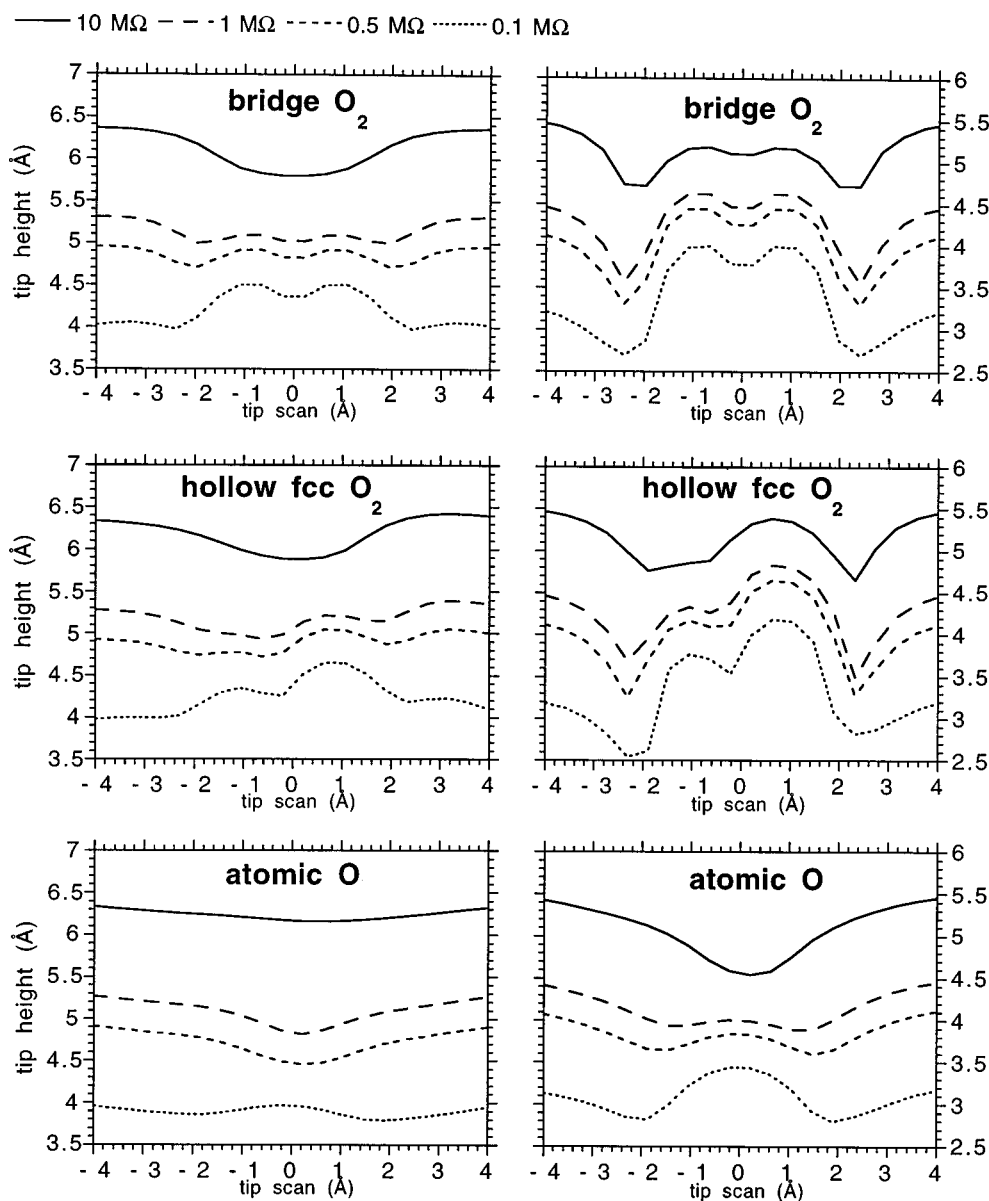


FIG. 7. Combined influence of the tip apex structure and tunnel gap resistance. Topographic scans along the O-O bond for different values: 10 M Ω (solid line), 1 M Ω (long dashed line), 0.5 M Ω (dashed line), and 0.1 M Ω (dotted line) for models of two contaminated tips: the O-terminated tip apex (left column), and the CO molecule adsorbed on the Pt tip apex (right column).

current value far from the molecule than in the case of Fig. 5. The through-surface depression is still present, and is even more marked than in the Pt apex case. However, the through-molecule current is strongly enhanced. It mainly corresponds to a contribution of the π^* orbital for the bridge site, and to a smaller extent for the hollow site. The decomposition of the current therefore is in concordance with the qualitative interpretation of the topographic scans given in Sec. IV.

Even if the contamination with O and CO yield qualitatively the same effect, these tips are not totally equivalent. In the case of the O atom, the tip body draws closer to the surface compared to the Pt tip, and the contamination can be seen as an additional scattering for the tunneling electrons which adds to the tunnel gap resistance. Therefore, for a given imposed total resistance the “true” tunnel resistance is smaller, yielding an amplification of the molecular contrast. For the CO contaminant, even if the O apex is much closer to

the surface, the tip body is moved further from the surface if the 3-Å distance between O and Pt apex is taken into account. The CO molecule at the tip adds a contribution to the current. Due to the low z of the CO molecule and its proximity to the adsorbate, this contribution is enhanced when the CO tip probes the O₂ molecule on the surface. The overall effects of both tips is to probe the surface wave function at a lower height, compared to the metallic tip.

This discussion, based on the reduced tip-adsorbate distance, can be completed by a more precise analysis of the character of the tip orbitals that participate in the tunneling. For the CO-terminated tip, the 5σ CO orbital is clearly the main contributor, as it is the case when CO is chemisorbed on the surface.²⁵ The 5σ CO orbital is directional, and can more efficiently probe the out-of-phase $2p_z$ lobes of the π^* O₂ orbital than the spherical Pt $6s$. Moreover, the molecular orbital energies are close, and both effects add to yield a very

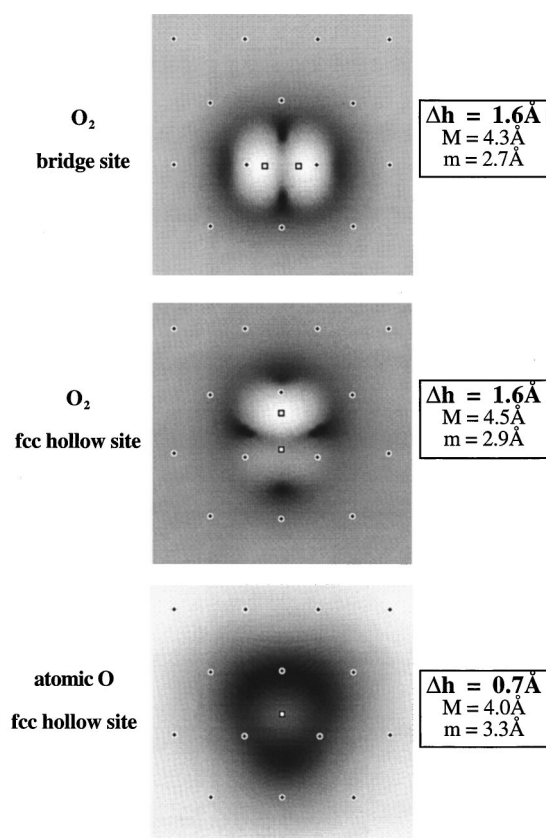


FIG. 8. 10×10 - \AA^2 STM topographic computed images (bias 10 mV, current 20 nA) with a CO molecule chemisorbed at the Pt tip apex. Minimum (m) and maximum (M) z values are given. Labels for the atom positions are the same as in Fig. 2. The black-to-white scale is associated with the minimum-to-maximum tip z values.

favorable interaction between the tip 5σ CO orbital and the O_2 π^* orbital on the surface. The situation of the O-terminated tip is somewhat intermediate between that of the CO and Pt tips, since tip contributions arise both from the O $2p_z$ orbitals and from the Pt $6s$ orbitals of the tip base. The more diffuse character of the Pt orbitals compensate for the atomic height difference at the tip apex. However, these metal and oxygen contributions to the tunnel current interfere destructively, which gives a weaker enhancement of the π^* O_2 current compared to the CO tip. Therefore, molecular-orbital features of a given adsorbate can be amplified in the tunnel current if tip states with small orbital expansion and adequate energy level can be selected at the tip apex. In our case, the π^* O_2 contribution is efficiently enhanced by a CO-terminated tip.

VI. CONCLUSION

Theoretical simulations of STM images of the various adsorption states of O_2 on Pt(111), characterized geometrically by previous spectroscopic studies and the *ab initio* local-spin-density calculations presented here, have been analyzed. Two molecular precursors are obtained—one chemisorbed on the bridge site, and the other chemisorbed on the hollow site—with very similar chemisorption energies, but the ex-

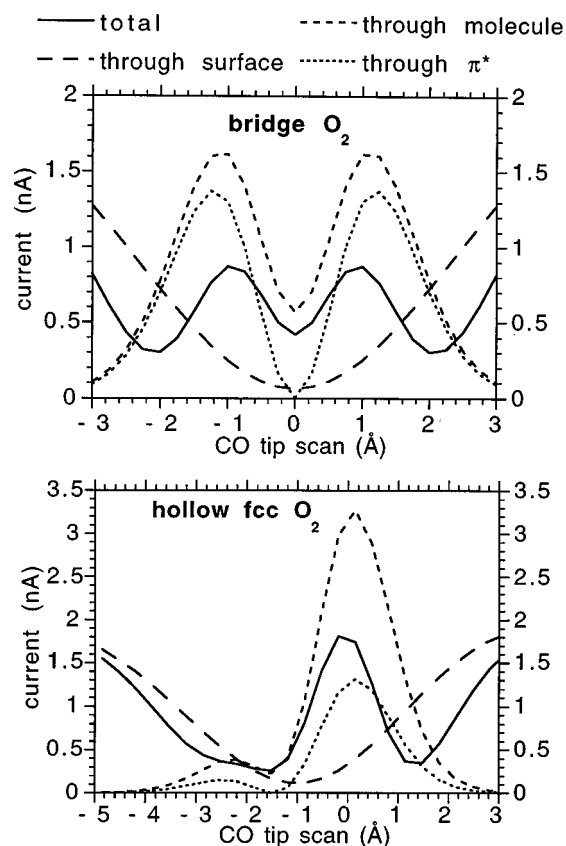


FIG. 9. Current (solid line) for a scan along the O-O direction centered on the molecule for a CO-terminated tip at a height of 5.3 \AA relative to the surface and for a bias voltage of 10 mV. The current is decomposed through surface (long dashed line), molecule (dashed line), and π^* molecular-orbital (dotted line) contributions.

perimental images, with positive features for the molecule, can only be reproduced if specific tip apices are chosen with some contamination and if the gap resistance is reasonably small.

Indeed, contamination at the tip apex either by O atoms or CO molecules gives a strong amplification of the molecular features in the images, since the surface wave function can be probed at a lower height. The molecule has two effects on the tunnel current: it decreases the through-surface contribution, but adds its own through-molecule current. This molecular contribution is dominated by the participation of the O_2 π^* orbital, which is in quasiresonance with the surface Fermi level due to its open-shell character. The calculations confirm that the STM is very sensitive to the precise coordination of the molecule to the surface, and represents an excellent tool to study elementary molecular processes at surfaces.

ACKNOWLEDGMENTS

The authors acknowledge support from the Spanish-French collaboration program PICASSO 98045. J.C. acknowledges financial support from the Spanish CICYT under Contract No. PB96-0916.

- * Author to whom correspondence should be addressed. FAX: (33) 4 72 44 53 99. Electronic address: sautet@catalyse.univ-lyon1.fr
- ¹P. S. Weiss and D. M. Eigler, *Phys. Rev. Lett.* **71**, 3139 (1993); P. Zeppenfeld, C. P. Lutz, and D. M. Eigler, *Ultramicroscopy* **42–44**, 128 (1992).
- ²A. C. Luntz, J. Grimblot, and D. E. Fowler, *Phys. Rev. B* **39**, 12 903 (1989); J. Grimblot, A. C. Luntz, and D. E. Fowler, *J. Electron Spectrosc. Relat. Phenom.* **52**, 161 (1990); C. T. Rettner and C. B. Mullins, *J. Chem. Phys.* **94**, 1626 (1991); W. Wurth, J. Stöhr, P. Feulner, X. Pan, K. R. Bauchspiess, Y. Baba, E. Hudel, G. Rocker, and D. Menzel, *Phys. Rev. Lett.* **65**, 2426 (1990).
- ³C. Puglia, A. Nilsson, B. Hernnäs, O. Karis, P. Bennich, and N. Martensson, *Surf. Sci.* **342**, 119 (1995).
- ⁴B. C. Stipe, M. A. Rezaei, W. Ho, S. Gao, and M. Persson, and B. I. Lundqvist, *Phys. Rev. Lett.* **78**, 4410 (1997).
- ⁵N. R. Avery, *Chem. Phys. Lett.* **96**, 371 (1983); D. A. Outka, J. Stohr, W. Jark, P. Stevens, J. Solomon, and R. J. Mdx, *Phys. Rev. B* **35**, 4119 (1987); H. Steininger, S. Lehwald, and H. Ibach, *Surf. Sci.* **123**, 1 (1982).
- ⁶P. Sautet, *Chem. Rev.* **97**, 1097 (1997), and references therein.
- ⁷A. W. E. Chan, R. Hoffmann, and W. Ho, *Langmuir* **8**, 1111 (1992); R.-H. Zhou and P.-L. Cao, *Phys. Lett. A* **169**, 167 (1992); B. Hellsing, *Surf. Sci.* **282**, 216 (1993).
- ⁸A. Eichler and J. Hafner, *Phys. Rev. Lett.* **79**, 4481 (1997).
- ⁹J. A. Nieminen and S. Paavilainen, *Surf. Sci.* **405**, L573 (1998).
- ¹⁰J. Tersoff and D. R. Hamann, *Phys. Rev. B* **31**, 805 (1985).
- ¹¹G. Kresse and J. Hafner, *Phys. Rev. B* **49**, 14 251 (1994).
- ¹²J. Furthmüller, G. Kresse, and J. Hafner, *Phys. Rev. B* **50**, 15 606 (1994).
- ¹³D. Vanderbilt, *Phys. Rev. B* **41**, 7892 (1990).
- ¹⁴J. P. Perdew, J. A. Chevary, S. H. Vosko, K. A. Jackson, M. R. Pederson, D. J. Singh, and C. Fiolhais, *Phys. Rev. B* **46**, 6671 (1992).
- ¹⁵N. D. Lang, *Comments Condens. Matter Phys.* **14**, 253 (1989).
- ¹⁶P. Sautet, *Surf. Sci.* **374**, 406 (1997).
- ¹⁷P. Sautet and C. Joachim, *Phys. Rev. B* **38**, 12 238 (1988); *Chem. Phys. Lett.* **185**, 23 (1991); *Surf. Sci.* **271**, 387 (1992); *Ultramicroscopy* **42–44**, 115 (1992).
- ¹⁸R. Hoffmann, *J. Chem. Phys.* **39**, 1397 (1963); for a review on applications of extended Hückel theory to surface science, see, for instance, R. Hoffmann, *Rev. Mod. Phys.* **60**, 601 (1988); M. Simonetta and A. Gavezzotti, *Adv. Quantum Chem.* **12**, 103 (1980).
- ¹⁹R. Landauer, *Philos. Mag.* **21**, 863 (1970).
- ²⁰J. Cerdà, M. A. Van Hove, P. Sautet, and M. Salmeron, *Phys. Rev. B* **56**, 15 885 (1997); J. Cerdà, A. Yoon, M. A. Van Hove, P. Sautet, M. Salmeron, and G. A. Somorjai, *ibid.* **56**, 15 900 (1997).
- ²¹E. Clementi and C. Roetti, *At. Data Nucl. Data Tables* **14**, 177 (1974); A. D. McLean and R. S. McLean, *ibid.* **26**, 197 (1981).
- ²²J. Silvestre and R. Hoffmann, *Langmuir* **1**, 621 (1985); A. W. E. Chan, R. Hoffmann, and W. Ho, *ibid.* **8**, 1111 (1992).
- ²³M.-L. Bocquet and P. Sautet, *Surf. Sci.* **415**, 148 (1998).
- ²⁴L. Bartels L., G. Meyer, and K. H. Rieder, *Appl. Phys. Lett.* **71**, 213 (1997).
- ²⁵M.-L. Bocquet and P. Sautet, *Surf. Sci.* **360**, 128 (1996).